

Design and simulation of railway vehicles braking operation using a scaled roller-rig

N. Bosso, A. Gugliotta & A. Somà

Politecnico di Torino, Dipartimento di Meccanica, Italy

Abstract

A 1:5 scale roller-rig has been recently realized at Politecnico di Torino for the simulation of railway dynamics. In this work it is shown that it is possible to reproduce the braking dynamics of a railway vehicle on the roller rig. For this purpose a disk-brake braking system has been designed that can be installed on the existing bogie. The inertia of the vehicle can easily be simulated adding inertia to the rollers, so that the braking distance can be evaluated on the basis of the angular displacement of the rollers. Design and optimisation of the system has been carried out with the aid of a numerical multibody model, in which different friction laws have been implemented. The simulations have been performed varying the running conditions (friction coefficient, axle load, velocity).

Keywords: wheel, rail, friction, roller-rig.

1 Introduction

A roller-rig is a test bench for railway vehicles, where the track is replaced by a pair of rollers for each wheelset of the vehicle. At Politecnico di a reduced scale roller rig (1:4 -1:5) Torino has been realized to perform dynamic simulations on a single wheelset or on an entire bogie. The realization of reduced scale models, lead to evident benefits in terms of costs of realization of the test rig and of the prototypes used to perform the tests. On the other hand it is necessary to use adequate similitude model to obtain, from the scaled results, an estimation of the behaviour of the real vehicle. Several models proposed in literature have been analysed and compared [1], and the vehicle has been designed according the similitude law proposed by Jaschinski [2].



The test rig has been initially designed to perform simulations to investigate running stability, to study the wheel-rail contact and to identify the dynamic behaviour of the vehicle. Design flexibility has soon evidenced the possible application to other field of investigation. In this work it is shown that it is possible to simulate, through a Roller-Rig, the braking dynamics for a vehicle. In this way it is possible to perform accurate analysis of variation of the friction coefficient, in a future stage of the project; the roller rig could be used to validate anti-skid systems and to test diagnostic systems which operate on railway vehicles.

In order to use the Test rig to carry on braking simulations, it is necessary first of all to realize the braking system on the bogie, furthermore it is necessary to reproduce the braked mass of the entire vehicle.

The braked mass of the vehicle can be simulated acting on the inertia moment of the rollers. Imposing that the tangential deceleration of the rollers, in braking condition, is equal to the vehicle deceleration, it is possible to calculate the inertia moment of a roller with radius R_R equivalent to a vehicle with braked mass M , as:

$$J_R = M \cdot R_R^2 \quad (1)$$

Since we want to simulate vehicles with axle load up to 25 tonnes (in 1:5 scale 200 kg/axle, it is possible to calculate an inertia equal to 6.48 kg m^2), and in order to reduce the rollers mass, the system has been designed using a gearbox with gear ratio 10, placed between the rollers and the additional inertia, as shown on figure 2 (6).

2 Numerical model

The numerical model has been realized using a Multibody code (MSC/Adams), according to the scheme shown on figure 1, where, regarding the longitudinal dynamic, a single axle has been considered.

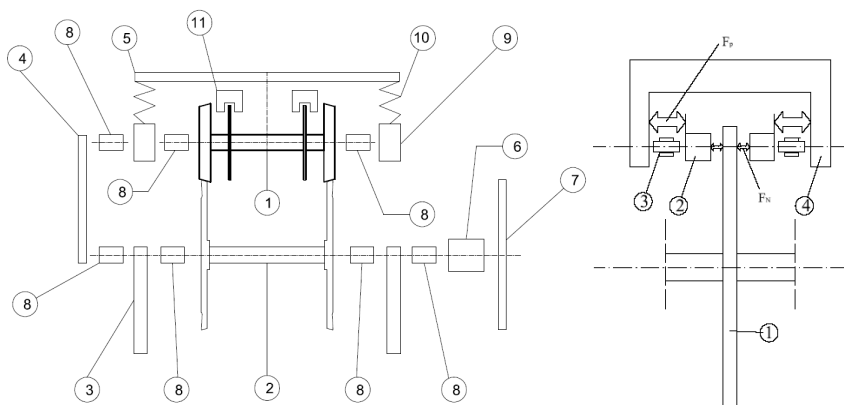


Figure 1: Multibody model scheme (left), brake system. detail.

The model is composed by the roller-rig, whose parts are the rollers supports (3) and the two rollers (2) connected by a rigid joint; the vehicle is made of one wheelset (1), connected to the bogie frame (5) by mean of the primary suspension stage (10) placed in correspondence of the axle bearing boxes (9). The bearings supporting the rollers and the wheelset have been simulated using rigid revolute joints (8). In order to reproduce the longitudinal curvature of the rollers, has been adopted the constraint scheme described in [3], composed by a mass-less dummy body (4), and by two revolute joints in order to keep fixed the distance between the rotational axis of rollers and wheelset. The braking system is made of two brake disks rigidly connected to the wheelset and by two calipers (11) connected to the bogie frame. In order to simulate the braked mass of the vehicle, this has been reported to the rollers axis, through a disk (7) and amplified by a gear-box (6). The gear box is required in order to reduce the disk mass and therefore the solicitations on the rollers supports.

The described system is brought to the test initial velocity by an electric motor connected to the left roller (where the additional inertial disk is not present) and decelerated by the braking system.

The braking system is simulated as shown on fig. 1 (right), where two pneumatic pistons (2) are allowed to slide respect the caliper (4) in lateral direction, due to the two cylindrical joints (3). The motion of the pistons is limited by the presence of the disk, by mean of a unilateral elastic force simulated as follows:

$$F_N = \begin{cases} 0 & \text{for } x \leq x_0 \\ K(x) \cdot (x - x_0) - C \cdot \dot{x} & \text{for } x > x_0 \end{cases} \quad (2)$$

where x_0 is the clearance between disk and brake pad and x, \dot{x} are respectively the displacement and velocity of the piston. The braking effort is actuated by the pressure p of the pneumatic circuit, which is imposed on the system as a temporal law to simulate the braking manoeuvre.

Among each piston and the caliper as been therefore applied a pneumatic force expressed by the law:

$$F_p = p \cdot A_p \quad (3)$$

Where the frictional effects on the seals have been neglected and A_p represents the area of the piston. The friction force acting between pad and disk, which produces braking efforts, depends on the normal force expressed by eq. 3, and has been described according to a non linear and numerically stable model, as described in [4], according the equation:

$$F_f = \frac{\omega_y^s \cdot r_b \cdot \chi}{\sqrt{1 + \left(\frac{\omega_y^s \cdot r_b \cdot \chi}{|F_N| \cdot \mu} \right)^2}} \quad (4)$$

where ω_y^s is the angular velocity of the wheelset, r_b is the average braking radius (located in the center of the brake pads), μ is the pad-disk friction

coefficient (0.4) and c is a parameter (10^6) used to express the disk and pad deformation in the adhesion region of the force-velocity diagram, in order to avoid the discontinuity caused by the Coulomb's law ($\chi = \infty$).

2.1 Wheel-roller contact

The wheel-roller contact model, has been described according to [3], but only the longitudinal creep component has been considered in this work, because in case of braking it assume a dominant role in the phenomena. This force can be expressed by:

$$F_{x,DS} = - \frac{f_{11} \cdot \xi_{R,L}}{\sqrt[n]{1 + \left| \frac{f_{11} \cdot \xi_{R,L} + f_{22} \cdot \eta_{R,L} + f_{23} \cdot \phi_{R,L}}{\mu \cdot N} \right|^n}} \quad (5)$$

where the f_{ij} terms are the creepage coefficients for the linear region of the characteristics, calculated according to the Kalker linear theory [5]; ξ , η , ϕ are the kinematical creepages of the right (R) and Left (L) wheel. During braking, the most important creepage term is the one related to the longitudinal direction ξ , while the others can be neglected. A simplified (first order) expression for the longitudinal creepage read:

$$\xi_{R,L} = \pm \left(\frac{b}{\omega_s \cdot r} + \frac{\lambda}{r} \cdot \frac{r+R}{R} \cdot y \right) - \frac{\omega_s \cdot r - \omega_r \cdot R}{\omega_r \cdot R} \quad (6)$$

where b represents the gauge, r and R the contact radii of wheel and rollers respectively, λ the profiles conicity, ω_s and ω_r the angular velocity of wheelset and roller.

Equation (6) has been described for conical profiles, in case of real profiles can be extended introducing the dependence of b , r , R , λ by the lateral position of the wheelset respect the track center line (in this case defined by the pair of rollers) as shown in [3]. In this work, the analysis has been limited to the case of conical profiles, since the influence of profiles non linearity (only affect the terms among brackets of expression (6) during braking results negligible).

2.2 Wheel /rail friction

Experimental analysis performed in braking conditions show that in this case a Coulomb friction model often results erratic. For this reason several authors, develop models where the friction coefficient vary as function of the sliding velocity, normal load and creepages.

The dependence of the friction coefficient from the sliding velocity v , has been proposed at first by Kraft [6], according to results from experimental tests. The equation proposed by Kraft is:

$$\mu = \mu_0 \cdot \left(1 - 0.5 \cdot e^{-0.138/|v|} - 0.5 \cdot e^{-6.9/|v|} \right) \quad (7)$$

Where μ_0 is the static friction coefficient. The sliding velocity, in case of pure longitudinal sliding, for the wheel-roller contact (equation(6)) can be expressed by:

$$v = \xi \cdot V = \xi \cdot \omega_R \cdot R \approx (\omega_R \cdot R - \omega_s \cdot r) \quad (8)$$

The first exponential term of the equation (7), cause a sharply reduction of the friction coefficient for little values of the sliding velocity, while the second terms assure a further reduction for higher values of the sliding velocity.

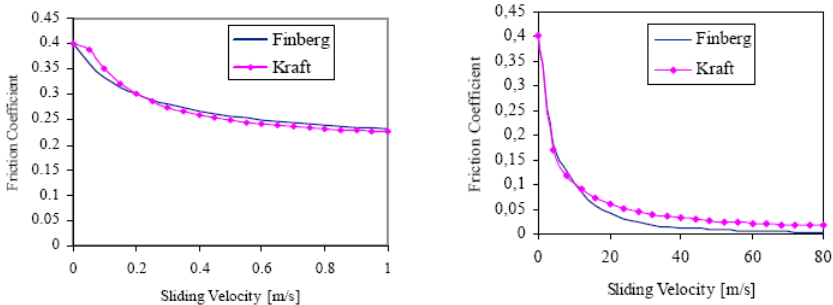


Figure 2: Behaviour of the friction coefficient according to the Kraft and Fingberg theory at low and high values of the sliding velocity.

Equation (7) was later modified by Fingberg [7], to obtain a better description of the phenomena at law sliding velocity:

$$\mu = \mu_0 \cdot \left(\frac{50}{100 + v^2} - \frac{0.1}{0.2 + |v|} \right) \quad (9)$$

The two formulations give similar results, but the Fingberg's approach is more suitable for lower sliding velocity where a more regular behaviour can be observed, Kraft's theory is more accurate at higher speed where friction coefficient evaluated using Fingberg's method vanish (see figure 2).

Periard [8] introduced two different empirical formulations as function of the sliding velocity of the wheel. The first is obtained from the experiments carried on by Poiré and Bochet of a wheel on a rail at a sliding velocity up to 20 m/s and is expressed by the relation:

$$\mu = \mu_0 \cdot \frac{1}{1 + 0.03 \cdot |v|} \quad (10)$$

The second is formulated according to the experiments of Galton [9] regarding sliding of a brake pad over a wheel during braking:

$$\mu = \mu_0 \cdot \frac{1 + 0.018 \cdot |v|}{1 + 0.097 \cdot |v|} \tag{11}$$

Both the laws show similar behaviours in the usual range of the sliding velocity (figure 3), however the friction coefficient using Galton’s method has an asymptotic trend at about 18% of the static value, while using the Periad’s method vanish.

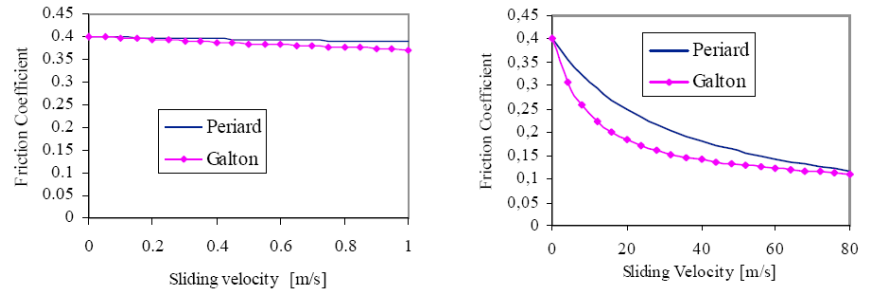


Figure 3: Friction coefficient behaviour according to the Methods of Poiré - Bochet and Galton using the description proposed by Periard.

3 Numerical analysis

Aim of this section is the analysis of the braking dynamics depending on the axle-load (12, 16 and 22.5 t/axle in real scale), of the friction coefficient (0.4, 0.2 and 0.15) and of the initial braking velocity (50, 100, 150 km/h in real scale). Numerical simulations are performed using the models described in the previous section (equation 5). All the numerical results are to be considered as referred to the reduced scale model. The results in real scale can be obtained applying the appropriate scaling factors [2]. At first a constant friction coefficient of 0.4 has been adopted, in this way has been possible to compare the results with those of analytical calculations.

Table 1: Braking times calculated analytically and numerically.

ω_0 [rpm]	ω' [rad/s]	t_i-t_s [s]	t_s [s]	t_a [s]
(v1) 1800	2.42	0.04	1.04	1.04
(v2) 3000	23.36	0.40	1.40	1.40
(v3) 6000	75.72	1.31	2.30	2.31
(v4) 12000	180.44	3.11	4.12	4.11

The vehicle has been braked starting from different initial velocity as shown on figure 3, After 4 seconds a pressure has been applied in order to reach the maximum braking force (imposed equal to 100 N) after 1 second.

The vehicle used for the simulations has rollers inertia equal to 0.1 kg m² and an average braking radius r_b equal to 0.0725 m. As shown on figure 4, up to a

certain time t_1 , the brake effort develops with increasing pressure and force, after the time t_1 the normal load reach its maximum (in this case equal to 100 N).

In Table 1 are indicated the rollers velocity at time t_1 , the time interval in which the braking took place at constant force (t_1 - t_s), the total brake time evaluated using the numerical (t_s) and the analytical model (t_a).

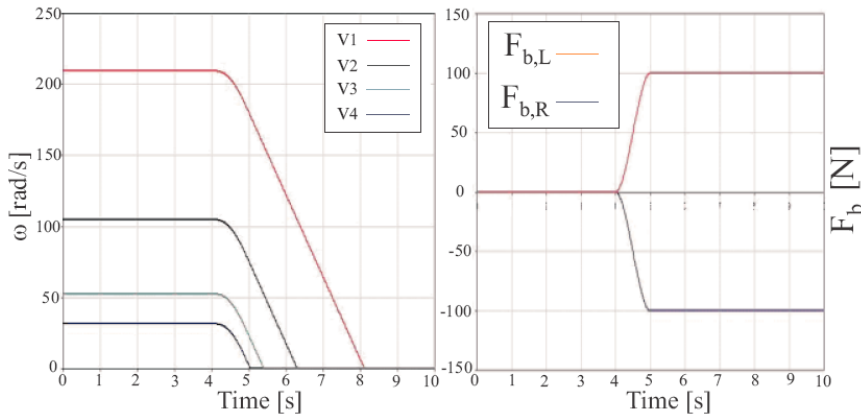


Figure 4: Rollers deceleration (left). Braking force behaviour (right).

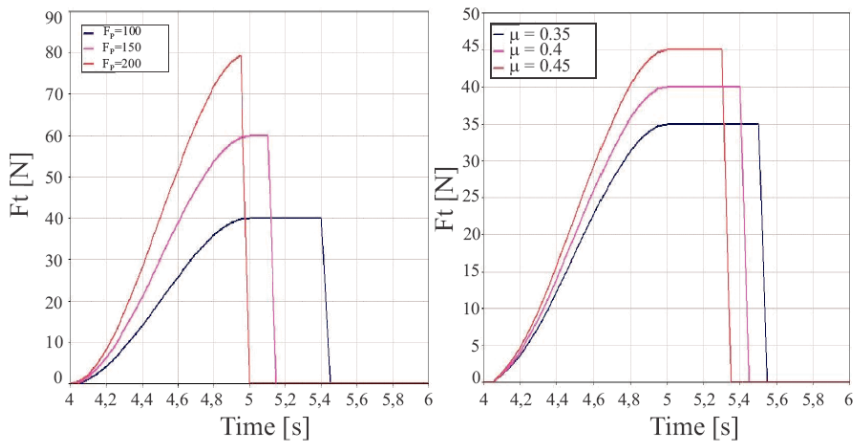


Figure 5: Friction force behaviour versus time as function of the normal load (left) and of the friction coefficient (right).

In order to evaluate the effect of the normal load and of the friction coefficient, a series of simulation has been performed starting from the velocity of 100 km/h in real scale, modifying the pressure on the calipers (100, 150, 200 N) with a friction coefficient of 0.4 as shown in figure 5 (left). Then (figure 5, right)

the normal load has been kept constant (100 N) and the friction coefficient has been modified.

Previous analyses don't consider the variation of the friction coefficient during braking. Next Fingberg's and Periard's theories will be introduced in order to evaluate this effect.

3.1 Comparison between different adhesion laws.

In this section the constant friction coefficient model will be compared with the models proposed by Periard (equation (13)) and Fingberg, according to equation (11). Fingberg's law is more suitable for low sliding velocity, while Periard's one is better at higher velocity.

Considering a braking manoeuvre with constant torque, the friction forces behaviour, shown on figure 6 (left), can be distinguished in three regions. In a first phase the friction force increase linearly together with the longitudinal creepage, during this phase the contact area is characterised by full adhesion. The second region shows a non linear increasing trend of the friction forces. This is due to the formation, in the contact patch of a portion where sliding occurs. The sliding portion gradually increases up to saturate the entire contact patch; when the entire area is in sliding condition, the maximum value of the tangential force is reached. This condition is also known as optimal adhesion condition.

Further increasing of the creepage, produce different effect depending on the considered model. Using the constant friction coefficient model, the maximum friction force remains constant.

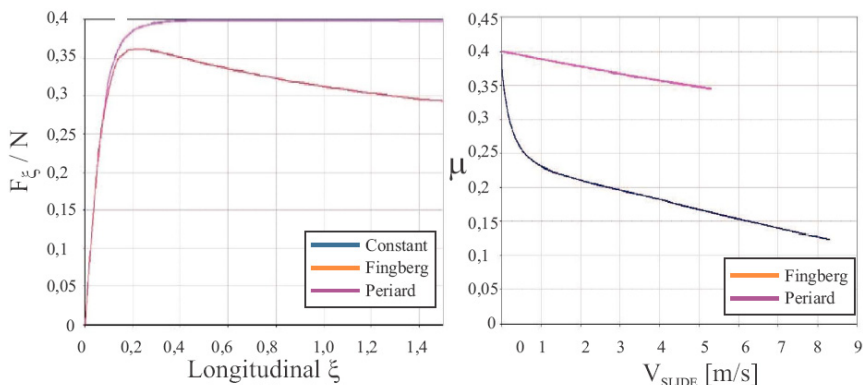


Figure 6: Comparison between different adhesion laws ($V=100$ km/h, $N=12$ t/axle): adimensional longitudinal creep force versus creepage (left); friction coefficient versus sliding velocity.

With Fingberg's and Periard's models, if the creepage increase over the maximum of adhesion, the friction force reduces. Periard's model shows a little reduction (for small creepage) respect the constant model, while Fingberg's model predict an important reduction in the same conditions.

Table 2: Comparison between different adhesion laws: $N = 96 \text{ kg}$, $V = 100 \text{ Km/h}$.

Law	Cb [Nm]	$F_g / \mu N$ [/]	t_{stop} [s]	s_{stop} (1:5) [m]
Fingberg	32.46	0.984	4.85	43.44
Periard	35.61	0.99	4.54	41.43
μ constant	35.61	1.00	4.54	41.43

Analysing in detail the friction force behaviour, a different creepage value in correspondence of the optimal adhesion condition can be observed, equal to 0.27% using Periard's model, and 0.19% with Fingberg's.

The different value of the braking force lead obviously to higher stop time and distance with the Fingberg's model, as indicated on table 2.

As can be seen on figure 6 (right), the friction coefficient in full sliding condition is 0.345 with Periard's law and 0.134 using Fingberg's. This is related to the large discrepancies in the braking times and distances predicted by the two methods.

Using different methods, different peak values of the sliding velocity are reached starting from the same condition (initial velocity, braking torque).

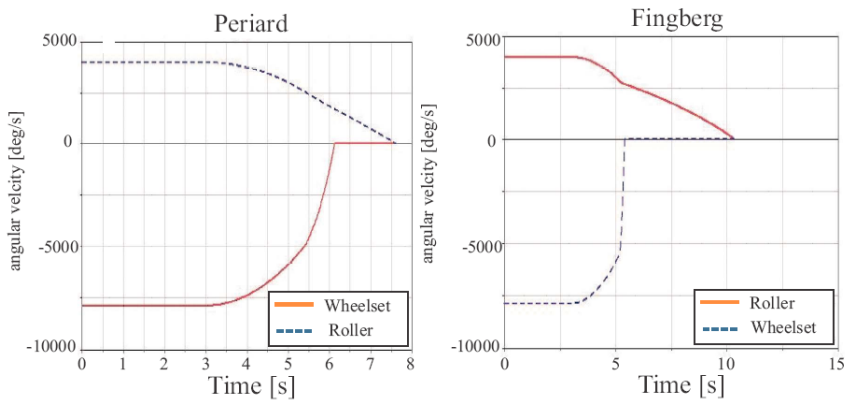


Figure 7: Wheel (solid) and roller (dashed) deceleration using Periard's (left) and Fingberg's (right) theory.

The time histories of the wheel and roller angular velocity, using the two approaches, shown on figure 7, allow a direct observation of the braking times.

According to the model of Fingberg, the braking time results to be 7.32 s, while using Periard's only 4.61 s are required to stop the vehicle (data in 1:5 scale). This means braking distances of 49.39 and 41.4 m using the two models.

Figure 7 shows the difference of the behaviour on roller respect to what can be expected on rails: when sliding occurs, the wheelset stops while the rollers continue their rotation, which represent, on rail, the longitudinal sliding of the vehicle.

3.2 Effect of the initial velocity

The dynamical behaviour during braking is strongly influenced by the initial velocity of the vehicle, due to the dependence of the friction coefficient by the sliding velocity.

Therefore, several simulations are performed on the previous analysed model (axle load 12 t: 96 kg in 1:5 scale) modifying the initial velocity: 50, 100 and 150 km/h (corresponding to angular velocity of the rollers equal to 34.5, 69 and 103.5 rad/s in 1:5 scale).

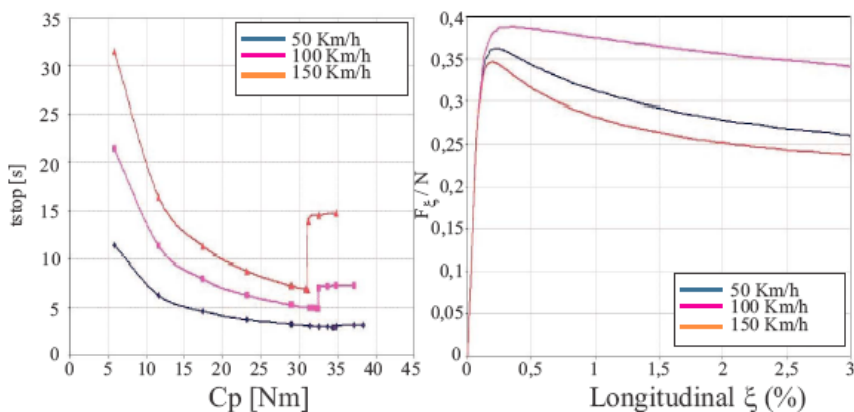


Figure 8: Stop times for different initial velocity as function of the brake torque. Adimensional creep force for different initial velocity.

Increasing the initial velocity, the maximum value of the sliding velocity increases and subsequently the friction coefficient decreases.

Therefore, performing the test with different values of the normal force acting on the brake pads (defining the brake torque), sliding occurs for high speed braking at high torque values (figure 8, left). Further increasing of the normal pressure is not useful for the stop time and distances.

On table 4, braking times and distances are indicated for different initial velocity and braking torque. The darkened fields in the table show an increment of the brake distance due to an increased torque; this means that sliding of the wheel has occurred.

Considering the longitudinal force as function of the creepage, can be observed that increasing the initial velocity, the optimal adhesion condition moves towards lower creepage values, as shown on figure 8 (right). This consideration has been quantified on table 4 and is important in order to design anti skid systems.

Table 3: Comparison between different adhesion laws: N = 96 kg.

Cb	V ₀ = 50 Km/h		V ₀ = 100 Km/h		V ₀ = 150 Km/h	
	t _{stop} [s]	s _{stop} [m]	t _{stop} [s]	s _{stop} [m]	t _{stop} [s]	s _{stop} [m]
5.8	11.38	42.3	21.43	147.7	31.52	316.3
11.6	6.28	26.4	11.34	84.5	16.38	174.3
17.4	4.61	21.0	7.98	63.37	11.33	126.9
23.2	3.77	18.2	6.30	52.7	8.815	103.1
29	3.27	16.5	5.29	46.2	7.30	88.7
30.74	-	-	-	-	6.96	85.5
30.97	-	-	-	-	6.916	85.1
31.03	-	-	-	-	6.906	85.0
31.09	-	-	-	-	13.93	150.5
31.32	3.12	15.9	4.98	44.3	-	-
31.90	-	-	4.93	43.9	-	-
32.25	-	-	4.88	43.6	-	-
32.36	-	-	4.86	43.5	-	-
32.46	-	-	4.85	43.4	-	-
32.48	3.05	15.7	7.02	47.6	14.46	157.7
33.64	2.99	15.5	7.22	47.9	-	-
34.22	2.96	15.34	-	-	-	-
34.45	2.95	15.3	-	-	-	-
34.68	2.93	15.26	-	-	-	-
34.74	2.93	15.4	-	-	-	-
34.8	3.13	15.3	7.27	49.4	14.73	161.3

Table 4: Comparison between different initial velocity: N = 96 kg.

V ₀ [Km/h]	ξ _{max} [%]	F _{ξ,Max} [N]	F _{ξ,Max} /μN
50	0.255	181.97	0.99
100	0.197	170.03	0.984
150	0.17	162.53	0.97

3.3 Brake at low friction coefficient

In the previous section a static friction coefficient of 0.4 has been considered, this value can be conventionally used in case of dry contact. It is well known that environmental effects (such as rain, ice, various contaminations) degrade the wheel rail friction. In this section different case are compared: normal condition ($\mu_0=0.4$), wet ($\mu_0=0.2$), and contemned contact ($\mu_0=0.14$).

Table 5: Optimal adhesion condition, different μ_0 .

μ ₀	ξ _{max} [%]	F _{ξ,Max} [N]	F _{ξ,Max} /μN
0.4	0.197	170.03	0.984
0.2	0.105	87.23	0.98
0.14	0.08	62.67	0.99



As shown on table 5, in reduced friction conditions, the optimal adhesion moves towards lower creepage values. This means that, in order to avoid skidding, it is necessary to reduce the braking torque.

Furthermore, as can be observed on figure 9, using a model with variable friction coefficient (Fingberg), and increasing the creepage, the friction coefficient decreases with the same law for each values of the initial friction.

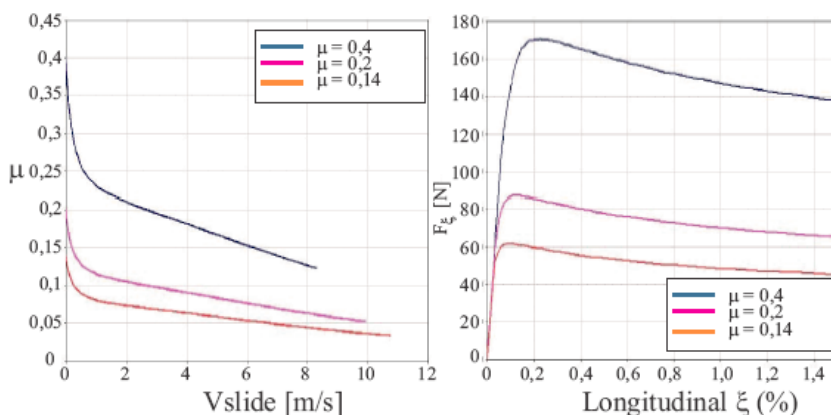


Figure 9: Friction coefficient (left) and creep force (right) for different surface condition: dry friction ($\mu_0=0.4$), wet (0.2) and contaminated (0.14).

This situation appear to be un-realistic, in fact it is difficult to believe that physical laws valid for direct contact between two elastic solids (wheel and rail) are not significantly altered by the presence of a third element among them. The problem could be further emphasized in case of long last at high sliding velocity. Therefore the analyses here illustrated are to be considered as a starting point, to be modified on the basis of further experimental tests. Test performed on roller rig could be useful for a better understanding of this phenomenon, due to the possibility to easily change and identify all the parameters.

3.4 Effect of the axle load

Finally the influence of axle load on brake dynamics is considered. Three load conditions are simulated: 12, 16 and 22.5 t/axle, corresponding to 96,128 and 180 kg in 1:5 scale.

Simulations are performed for different initial velocity values as shown in table 6, where are reported: the torque required to brake in optimal adhesion condition (C_b), deceleration, brake time and distance.

As can be noticed from figure 10 (left), the creep force is linearly proportional to the normal load except for a little variation of the optimum of adhesion (towards higher creepage values for higher loads).

Table 6: Effect of the axle load.

V_0 [m/s]	M [kg]	C_b [Nm]	t_{stop} [s]	s_{stop} [m]	\ddot{x} [m/s ²]
6.21	96	34.74	2.93	15.25	3.7
	128	46.40	2.92	15.2	3.72
	180	66.58	2.93	15.23	3.71
12.42	96	32.47	4.84	43.44	3.46
	128	43.21	4.84	43.44	3.47
	180	61.54	4.87	43.64	3.44
18.63	96	31.03	6.9	84.97	3.3
	128	41.24	6.9	84.88	3.31
	180	58.6	7.0	85.6	3.28

This is more evident analyzing the behaviour of the brake torque in condition of optimum of adhesion as function of the axle load as shown in figure 10 (right).

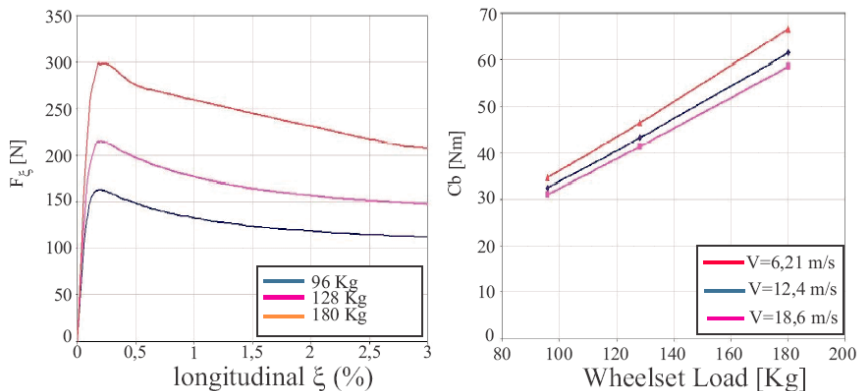


Figure 10: Braking force behaviour (Initial velocity 100 Km/h), as function of the creepage for different axle load (left), and torque in optimal adherence condition as function of the axle load for different initial velocity (right).

4 Design

The brake system is composed by two disks mounted on each wheelset (fig 11) fixed to the wheel by mean of two cylinders (2 and 3 in figure 11). The brake effort is exerted by two motorcycle type calipers (Brembo P32G) acted by air instead of oil. Experimental tests performed on this caliper demonstrate the possibility to achieve a linear regulation in the range 1-8 bar with braking efforts capable to reproduce the behaviour of the real vehicle (in scale). The calipers have been connected to the bogie frame with a beam system which integrates an estensimetric system to measure the braking force.

In order to measure the creepage, in the centre of the wheelset has been placed an incremental encoder.

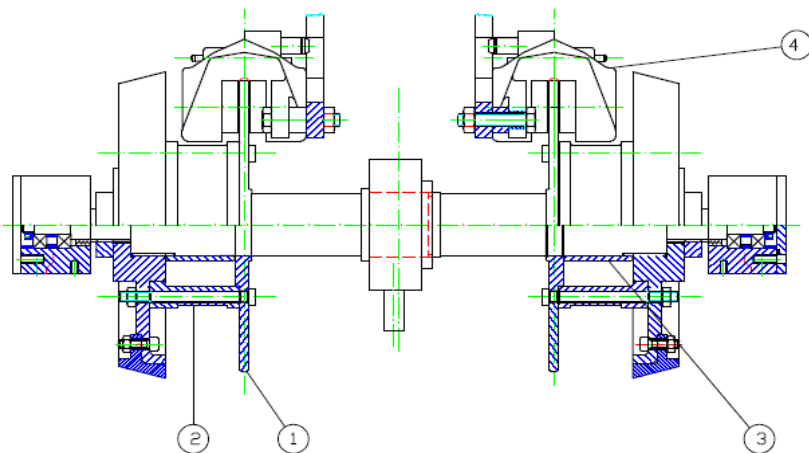


Figure 11: Drawing of the wheelset with brake disk(1) and calipers (4).

5 Conclusions

The work illustrate how is possible to use a Roller Rig in order to perform braking simulation on railway vehicles. In the first part of the work several friction laws, taken from literature are applied to a numerical model of a suspended wheelset on roller-rig in order to investigate braking dynamics.

The influence of different parameters is considered: friction coefficient, axle load, braking force and results of different theories are compared.

It is clear that different braking distance are predicted depending on the theory used, furthermore the behaviour of the friction coefficient in some conditions could not be fully explained in physical terms (figure 9).

For this reason the use of a test stand, as a Roller-Rig, under well known environmental condition can be useful to improve the modelling of the friction coefficient behaviour during braking.

The simulation has been used in the design phase of the braking system, to be applied to the existing Roller-Rig. Design has been performed in order to be able to simulate braking manoeuvre of vehicles with axle load up to 25 t/axle, and speed up to 400 km/h.

The experimental tests could be used both to investigate the friction coefficient behaviour, but also to develop more efficient anti-skid systems.

References

- [1] N. Bosso, A. Gugliotta, A. Somà, "Comparison of different scaling techniques for the dynamics of a bogie on roller rig"- Vehicle System Dynamics 37 (SUPPL.), pp. 514-530, 2003.

- [2] Jaschinski A., 1990, "On the application of similarity laws to a scaled railway bogie model.", DLR Institut für Dynamik der flugsysteme, Oberpfaffenhofen (Germania).
- [3] N. Bosso, A. Gugliotta, A. Somà, "Introduction of a wheel-rail and wheel-roller contact model for independent wheels in a Multibody code." – ASME/IEEE Joint Rail Conference, Washington, DC, 22-24 April 2001.
- [4] "Dry friction models", J.B. Ayasse, S. Iwnicki, H. Chollet, poster paper, XVIIth IAVSD Symposium, Lyngby, Denmark, 2001.
- [5] Kalker, J.J.: Three-dimensional elastic bodies in rolling contact, Kluwer Academic Publisher, 1990.
- [6] K. Kraft, "Der Einfluss der Fahrgeschwindigkeit auf den Haftwert zwischen Rad und Schiene.", Archiv für Eisenbahntechnik 22, 58-78, 1976.
- [7] U. Fingberg, "A model of wheel-rail squeal noise." Journal of sound and vibration 143, 365-377. 1990.
- [8] F. Periard. "Wheel-rail noise generation: curve squealing by trams." PhD thesis, TU Delft 1998.
- [9] G. Galton. "The action of brakes. On the effect of brakes upon railway trains." Engineering 25, 469-462. 1878.
- [10] D.J. Thompson, A.D. Monk-Steel, C.J.C. Jones, P.D. Allen, S. S. Hsu, S.D. Iwnicki, "Railway Noise: curve squeal, Roughness Growth, Friction and Wear", Rail research UK, June-2003.

